Supplementary Information (SI) for Sustainable Energy & Fuels.

Supporting Information

Cr_3C_2/Cr_2O_3 Dual-Phase Surface Engineering of Graphite Felt for Enhanced Conductivity and Catalytic Activity in Vanadium Redox Flow Batteries

Hao Tung Lin[1*], Shu-Mei He[1], Liang-Hong Liu[1] and Li-Tao Teng[1]

1 Industrial Technology Research Institute, Green Energy and Environment Research Laboratories, Tainan 711010, Taiwan

*(Corresponding author: htline2002@gmail.com)

(1). Effect of Chromium Precursor Concentration on Cr_3C_2 Formation

To examine the effect of chromium precursor concentration on carbide formation, additional samples were prepared using $Cr(NO_3)_3 \cdot 9H_2O$/EtOH solutions with concentrations of 0.4, 0.8, and 1.6 g/100 mL, denoted as CB-0.4, CB-0.8, and CB-1.6, respectively. As shown in Fig. S1, discernible Cr_3C_2-related reflections were only observed for CB-1.6, whereas no clear Cr_3C_2 diffraction peaks were detected for CB-0.4 or CB-0.8. Therefore, the 1.6 g/100 mL condition was selected for further investigation in the main study.

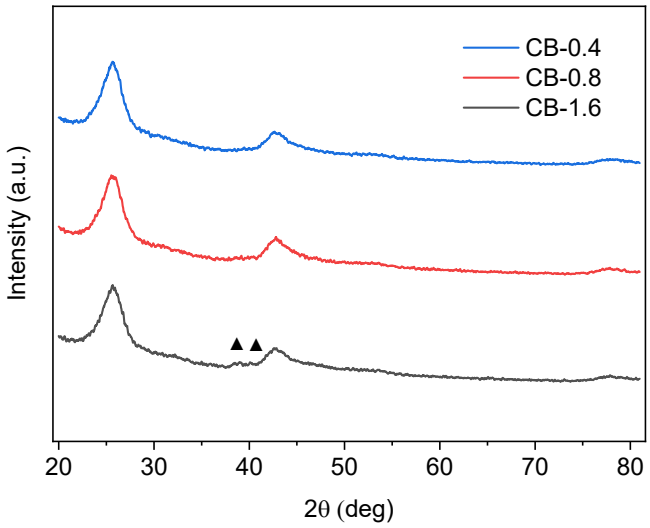

Fig. S1. XRD patterns of CB-0.4, CB-0.8, and CB-1.6 samples prepared using $Cr(NO_3)_3 \cdot 9H_2O$/EtOH precursor concentrations of 0.4, 0.8, and 1.6 g/100 mL, respectively.

Discernible Cr_3C_2-related reflections were observed only for CB-1.6.

(2). Estimation of Cr-Particle Surface Coverage

Based on the 2D projected image in Fig. 3b, the apparent surface coverage of the Cr-derived particles was estimated to be approximately 3–4%. It should be noted that this value represents only an image-based approximation and should not be interpreted as the true three-dimensional coverage of the porous graphite felt substrate. This is because graphite felt has a highly porous fibrous structure, and its cylindrical fibers can introduce projection-related errors when estimating particle coverage from a two-dimensional image.

(3). Vibrational Spectroscopic Characterization (FTIR and Raman)

As shown in Fig. S2, OX exhibits discernible Cr_2O_3-related vibrational features in both the FTIR and Raman spectra, consistent with the formation of an oxide-rich surface after oxidation treatment. By contrast, no clearly resolved Cr_2O_3-related signals are observed for CB+HPZ, suggesting that the oxide formed during the HPZ treatment is too thin and/or surface-confined to be effectively detected by these vibrational spectroscopic techniques. This interpretation is consistent with the TEM observation in Fig. 4, which reveals a thin chromium oxide shell on the carbide-modified surface. In addition, the XPS results in Figs. 6 and 7 further support the presence of Cr–O species and renewed oxygen-containing surface functionalities after HPZ.

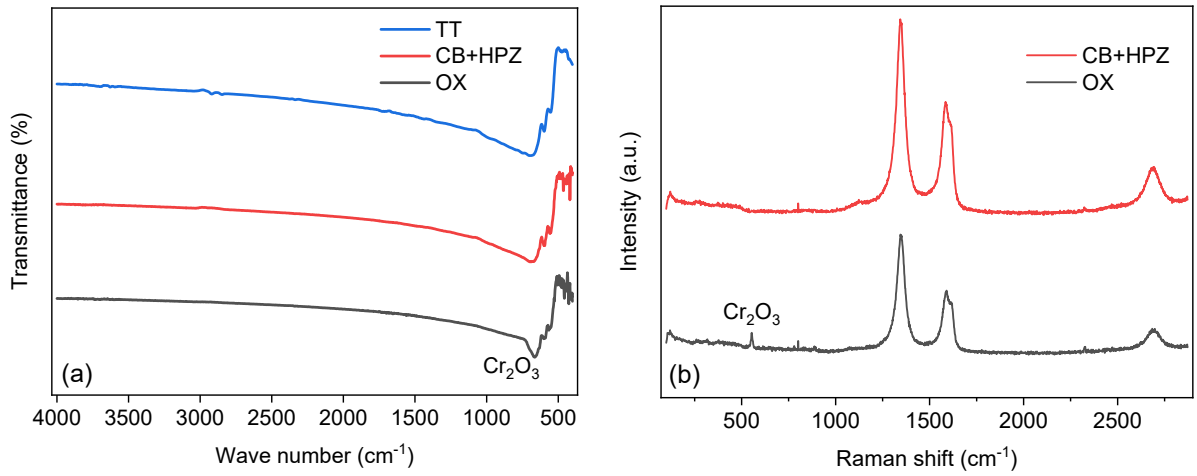

Fig. S2. (a) FTIR spectra of TT, CB+HPZ, and OX electrodes and (b) Raman spectra of

CB+HPZ and OX electrodes.

(4). Post-Cycling Morphological and Elemental Characterization

As shown in Fig. S3(a), particulate features remain visible on the graphite fiber surface after 200 cycles at 100 mA cm^{-2}, and no obvious large-scale particle detachment or structural collapse is observed. The corresponding EDS elemental maps confirm that Cr signals are still localized at the retained particulate regions (Fig. S3(b)), indicating that the chromium-derived species remain attached to the graphite felt fibers after prolonged cycling. The O signal partially overlaps with the Cr-containing regions (Fig. S3(c)), suggesting the presence of oxidized chromium species and/or surface oxygen functionalities. The C map (Fig. S3(d)) reflects the underlying graphite felt framework. In addition, V and S signals are detected over the electrode surface (Fig. S3(e, f)), which are attributed to residual vanadium electrolyte species and sulfate-containing electrolyte residues after cycling. The EDS spectrum in Fig. S3(g) further confirms the coexistence of C, O, Cr, V, and S signals. The quantitative EDS composition in Fig. S3(h) further shows that carbon is the dominant element, while a detectable Cr content remains after cycling. Overall, these post-cycling SEM/EDS results support the retention of chromium-containing particles on the graphite felt surface and are consistent with the stable cycling performance observed over 200 cycles.

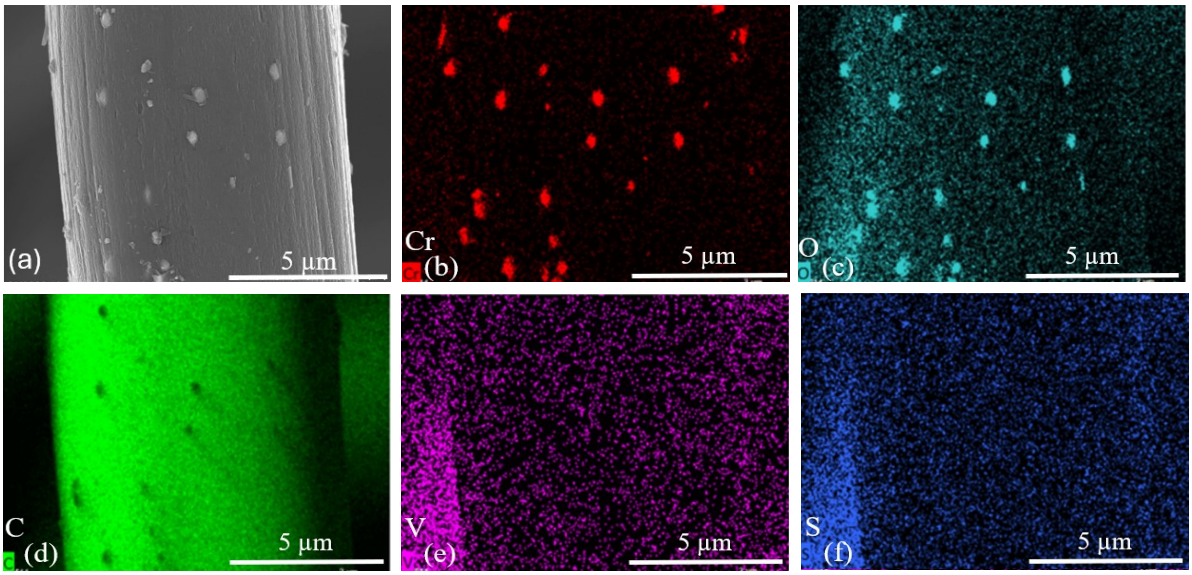

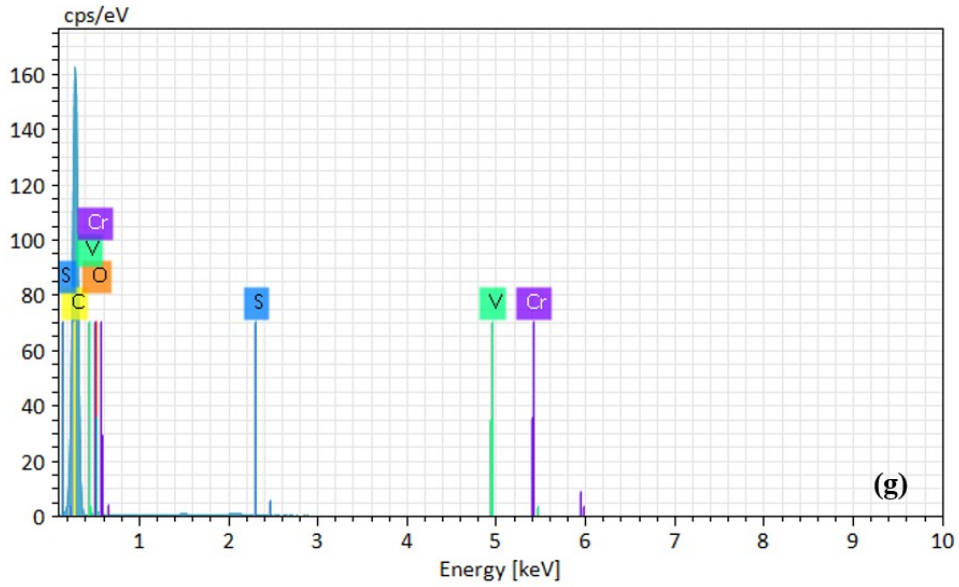

Element	Atomic number	Net counts	Norm. mass concentration /%	Norm. atomic concentration /%
C	6	302446	96.75	98.66
O	8	989	1.04	0.8
S	16	528	0.19	0.07
V	23	120	0.23	0.06
Cr	24	680	1.79	0.42
Total	□	□	100	100

(h)

Fig. S3. (a) Post-cycling SEM image of the CB+HPZ electrode after 200 cycles at 100 mA cm^{-2}. **(b–f)** EDS elemental mapping images of Cr, O, C, V, and S, respectively. **(g)** Corresponding EDS spectrum. **(h)** EDS elemental composition of the modified graphite felt electrode after VRFB cycling.

(5). Electronic resistance measurement of graphite felt electrodes

Four-point probe resistance measurements were performed using a CT 5601-Y system (QUATEK, Taiwan) to compare the relative electronic conduction of the Org, CB+HPZ, and

OX graphite felt electrodes. As summarized in Table S1, the Org sample showed an average resistance of 116.6 mΩ, whereas CB+HPZ exhibited a slightly lower average resistance of 109.6 mΩ. In contrast, OX showed a higher average resistance of 139.6 mΩ.

The lower resistance of CB+HPZ is consistent with the formation of conductive chromium carbide domains on the graphite fibers, whereas the higher resistance of OX suggests that the oxide-rich surface introduces additional electronic resistance. It should be noted that graphite felt is a porous three-dimensional fibrous network; therefore, the measured values may be affected by fiber-to-fiber contact, compression state, probe position, and complex current pathways. These measurements are therefore used mainly to compare the relative resistance trend among the samples, rather than to represent absolute intrinsic conductivity or strict sheet resistance.

Table S1. Four-point probe resistance values measured for Org, CB+HPZ, and OX graphite felt electrodes.

Sample	Four-point probe resistance (mΩ)	Average (mΩ)
Org	121, 118, 119, 114, 111	116.6
CB+HPZ	115, 112, 111, 108, 102	109.6
OX	139, 131, 144, 122, 162	139.6